



Review

A Comprehensive Review of Rubber Contact Mechanics and Friction Theories

Raffaele Stefanelli 1,* , Gabriele Fichera 2,* , Andrea Genovese 1 , Guido Napolitano Dell'Annunziata 1 , Aleksandr Sakhnevych 1 , Francesco Timpone 1 and Flavio Farroni 1

- Department of Industrial Engineering, University of Naples Federico II, 80125 Naples, Italy; andrea.genovese2@unina.it (A.G.); guido.napolitanodellannunziata@unina.it (G.N.D.); ale.sak@unina.it (A.S.); francesco.timpone@unina.it (F.T.); flavio.farroni@unina.it (F.F.)
- Department of Civil Engineering and Architecture, University of Catania, 95123 Catania, Italy
- * Correspondence: raffaele.stefanelli@unina.it (R.S.); gabriele.fichera@unict.it (G.F.)

Abstract

This review surveys theoretical frameworks developed to describe rubber contact and friction on rough surfaces, with a particular focus on tire-road interaction. It begins with classical continuum approaches, which provide valuable foundations but show limitations when applied to viscoelastic materials and multiscale roughness. More recent formulations are then examined, including the Klüppel-Heinrich model, which couples fractal surface descriptions with viscoelastic dissipation, and Persson's theory, which applies a statistical mechanics perspective and later integrates flash temperature effects. Grosch's pioneering experimental work is also revisited as a key empirical reference linking friction, velocity, and temperature. A comparative discussion highlights the ability of these models to capture scale-dependent contact and energy dissipation while also noting practical challenges such as calibration requirements, parameter sensitivity, and computational costs. Persistent issues include the definition of cutoff criteria for roughness spectra, the treatment of adhesion under realistic operating conditions, and the translation of detailed power spectral density (PSD) data into usable inputs for predictive models. The review emphasizes progress in connecting material rheology, surface characterization, and operating conditions but also underscores the gap between theoretical predictions and real tire-road performance. Bridging this gap will require hybrid approaches that combine physics-based and datadriven methods, supported by advances in surface metrology, in situ friction measurements, and machine learning. Overall, the paper provides a critical synthesis of current models and outlines future directions toward more predictive and application-oriented tire-road friction modeling.

Keywords: contact mechanics; tire friction; local contact area; road roughness; viscoelasticity



Academic Editor: John D. Clayton

Received: 2 October 2025 Revised: 21 October 2025 Accepted: 28 October 2025 Published: 29 October 2025

Citation: Stefanelli, R.; Fichera, G.; Genovese, A.; Napolitano Dell'Annunziata, G.; Sakhnevych, A.; Timpone, F.; Farroni, F. A Comprehensive Review of Rubber Contact Mechanics and Friction Theories. *Appl. Sci.* 2025, 15, 11558. https://doi.org/10.3390/ app152111558

Copyright: © 2025 by the authors. Licensee MDPI, Basel, Switzerland. This article is an open access article distributed under the terms and conditions of the Creative Commons Attribution (CC BY) license (https://creativecommons.org/licenses/by/4.0/).

1. Introduction

Tires are the key functional link between a vehicle and the road, transmitting the forces that enable acceleration, braking, steering, and stability. Their performance directly affects handling, comfort, safety, and energy efficiency. At the core, tire behavior is governed by the interaction between rubber and the rough road surface, which determines the available grip. Understanding this interaction requires a solid foundation in contact mechanics and friction theory [1–5].

Beyond tire-road applications, closely related rubber-shell interactions occur in frictional dampers, shell-type shock absorbers, and elastomeric elements radially confined

within curved housings. In these systems, contact mechanics controls local conformability and energy dissipation under confinement/curvature. Both analytical models (e.g., interaction of elastomeric fillers with open shells; structural damping in shell shock-absorber friction modules) and numerical studies (e.g., simulation of novel frictional dampers; adaptive behavior of shell-type elastic elements for drilling shock absorbers) show how viscoelastic contact principles extend to curved geometries [6–9].

Contact mechanics, a core discipline of tribology, investigates how solid bodies interact when in contact, whether under static or dynamic conditions [10–15]. Rooted in materials science and continuum mechanics, it provides a framework to analyze deformation under load, the distribution of stresses and pressures at interfaces, and the emergence of frictional forces [16–19]. High local stresses often develop at contact points, which may lead to fracture, yielding, fatigue, or wear. A key concept is therefore the determination of contact pressure, strongly influenced by geometry, material properties, and applied load [20–23]. Adhesion also plays a significant role, as intermolecular attraction between surfaces contributes to static friction, energy dissipation, and wear, particularly in soft materials such as rubber [24–27].

In practice, tire–road interfaces involve surfaces with pronounced roughness and curvature, resulting in highly localized contacts. The actual contact area is much smaller than the nominal footprint, generating elevated stresses and complicating friction prediction. For rubber, the degree of penetration into road asperities is critical, as it controls both hysteretic energy loss and adhesion [28–30]. This effect is commonly quantified by the ratio of real to nominal contact area (A_c/A_0) , where A_0 is the projected footprint and A_c is the true contact area. This ratio links surface roughness, rubber viscoelasticity, and loading conditions and is widely used in predictive friction models.

Ultimately, an accurate description of the A_c/A_0 ratio is central to understanding interfacial phenomena such as thermal and electrical resistance, adhesion, wear, and frictional behavior [31,32]. Modern contact theories therefore integrate realistic topographies, viscoelastic material response, and load dependence to provide a more reliable description of tire–road interaction.

2. Overview of Contact Mechanics

Classical contact mechanics established the analytical foundations for describing stresses, deformations, and real contact areas under load. Although developed for smooth, elastic bodies, these models remain the starting point for modern extensions to rough and viscoelastic surfaces. The most influential formulations include Hertz's solution for elastic contact, statistical models that incorporate surface roughness, and adhesive theories that account for intermolecular forces.

2.1. Hertzian Contact Theory

The foundation of modern contact mechanics can be traced to Heinrich Hertz's seminal work in 1882 [33]. Hertzian theory describes the localized stresses and deformations that arise when two elastic, axisymmetric, parabolic bodies are pressed together under a normal load [33–35]. It provides closed-form expressions for contact area, pressure distribution, and surface displacements as a function of applied force, radii of curvature, and elastic properties. Importantly, the solution applies to non-adhesive contacts, where no tensile stresses occur in the contact patch. Despite its assumptions, Hertzian theory remains a cornerstone for more advanced models.

Although originally derived for parabolic geometries, Hertzian solutions remain accurate when applied to practical cases such as sphere–sphere and cylinder–cylinder contact [36–38]. In these cases, theoretical point or line contacts are replaced by finite contact

areas due to elastic deformation, leading to so-called Hertzian contact stresses [39,40]. The theory assumes small deformations, an unchanged geometry, and a purely elastic response. For two cylinders, the pressure distribution is nearly parabolic, peaking at the center, where the maximum contact pressure p_{max} occurs, and vanishing at the edges.

A simplified yet widely used configuration is the indentation of an elastic half-space by a rigid sphere, illustrated in Figure 1.

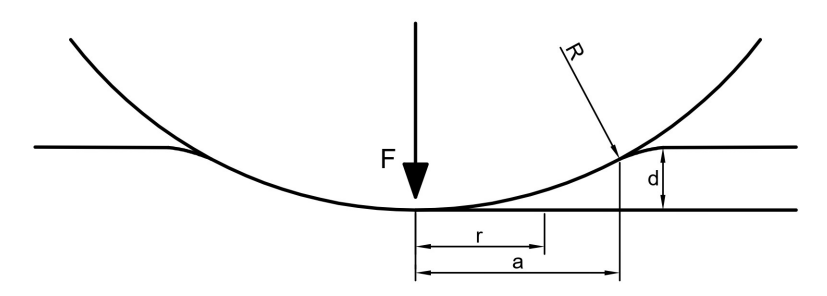


Figure 1. Elastic half-space indented by a rigid sphere of radius *R* [20].

In this case, the indentation depth d and the contact radius a can be expressed analytically in terms of the load F, sphere radius R, and effective elastic modulus E^* .

The principal Hertzian equation for a spherical elastic body indenting on an elastic half-space is reported in [20,26]. Assuming a quadratic pressure distribution:

$$p(r) = p_{max}\sqrt{1 - \frac{r^2}{a^2}}, \quad r \le a, \tag{1}$$

the resulting force-displacement relationship takes the form

$$F = \frac{4}{3}E^*R^{1/2}d^{3/2},\tag{2}$$

from which the key Hertzian expressions follow:

$$a = \left(\frac{3FR}{4E^*}\right)^{1/3}, \qquad p_{max} = \left(\frac{6FE^{*2}}{\pi^3 R^2}\right)^{1/3}.$$
 (3)

The effective elastic modulus E^* accounts for the properties of both bodies:

$$\frac{1}{E^*} = \frac{1 - \nu_1^2}{E_1} + \frac{1 - \nu_2^2}{E_2},\tag{4}$$

where E_i and v_i are Young's modulus and Poisson's ratio of body i.

Figure 2 further illustrates the quadratic pressure distribution under increasing vertical loads, showing how the maximum pressure grows while the contact radius expands accordingly.

Although Hertz and subsequent extensions by Sneddon [41,42] did not account for adhesion, this framework remains the analytical basis for many modern models of rough surface contact, where asperities are idealized as spherical indenters on an elastic half-space.

Appl. Sci. 2025, 15, 11558 4 of 26

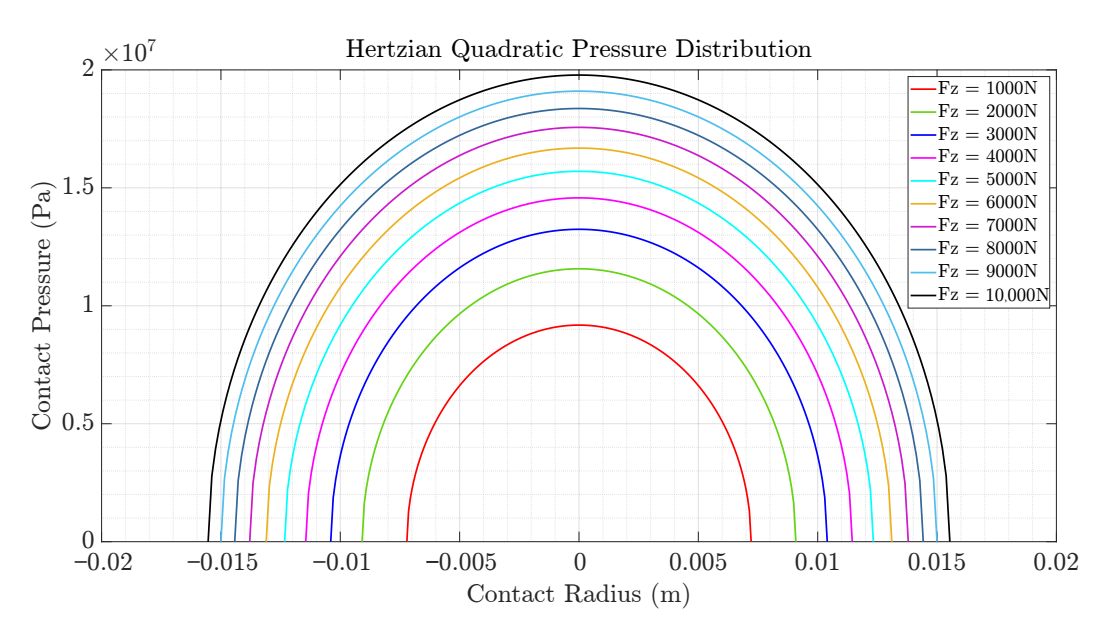


Figure 2. Quadratic pressure distribution of Hertzian contact under different vertical loads.

2.2. Surface Roughness in Contact Mechanics

Incorporating surface roughness into contact models presents a major challenge, given the stochastic and multiscale nature of real topographies [43–45]. A common approach is to describe rough surfaces as ensembles of asperities, each treated individually using Hertzian contact mechanics [46].

The pioneering work of Bowden and Tabor (1939) revealed that the real contact area between two rough surfaces is only a fraction of the nominal footprint [47]. Their observations demonstrated that asperity-level interactions dominate the stress distribution and can induce yielding or failure [16], establishing the basis of modern tribology [48–51].

Building on this paradigm, Archard [52–54] explained the experimentally observed linear relation between real contact area and applied load, which the classical Hertzian theory could not capture. He proposed a multi-asperity model where overall contact arises from the superposition of many Hertzian microcontacts, with the number of asperities scaling linearly with load. Archard also recognized the inherently multiscale nature of roughness [55,56], anticipating later fractal descriptions [57–61].

Following Archard, Greenwood and Williamson (1966) and Bush et al. (1975) provided rigorous mathematical frameworks for statistical modeling of rough surfaces [20,22,62,63]. The Greenwood–Williamson (GW) model is particularly influential, describing a rough surface as a population of spherical asperities with identical radii but randomly distributed summit heights. Each asperity deforms independently under Hertzian theory, and the overall contact is obtained by integrating the contributions of all asperities [64–67]. At its core, the GW model assumes that the asperities deform independently and that their summits are spaced sufficiently apart to neglect mutual interactions [68].

For rubberlike materials, the assumption of identical, non-interacting spherical asperities introduces some inaccuracies because the large compliance of the polymer causes neighboring contact spots to elastically interact through overlapping deformation fields. Finite-element and boundary-element analyses have shown that this simplification can overestimate the real contact area by 20–40% under typical tire–road pressures and underestimate the local peak stresses by a similar factor.

As illustrated in Figures 3 and 4, the spherical asperities higher than the mean separation *d* contribute to the contact.

Appl. Sci. 2025, 15, 11558 5 of 26



Figure 3. Contact between a rigid plane and a nominally flat but rough surface. Only asperities taller than the separation *d* contribute to load support [69].



Figure 4. Schematic representation of the Greenwood-Williamson statistical asperity model [69].

The contact radius a_i , area A_i , and load F_i of a single asperity with height z are

$$a_i = \sqrt{R(z-d)}, \qquad A_i = \pi R(z-d), \qquad F_i = \frac{4}{3}E^*R^{1/2}(z-d)^{3/2},$$
 (5)

where E^* is the effective elastic modulus (Equation (4)).

The total real contact area and load follow from integration over the asperity height distribution $\phi(z)$:

$$A_c = \pi NR \int_d^\infty (z - d)\phi(z) \, dz, \qquad F = \frac{4}{3} E^* N R^{1/2} \int_d^\infty (z - d)^{3/2} \phi(z) \, dz, \tag{6}$$

where N is the total number of asperities. Introducing the surface density η with $N = \eta A_0$, Greenwood and Williamson expressed these integrals in terms of the normalized separation $t = d/\sigma$ and the dimensionless functions $F_n(t)$:

$$F_n(t) = \int_t^\infty (z - t)^n \phi^*(z) \, dz,\tag{7}$$

where $\phi^*(z)$ is the standardized distribution [20,62].

The GW model thus links microscopic roughness features to macroscopic contact parameters such as load and real contact area, providing a powerful statistical framework that remains widely used in analytical and computational tribology [70–73].

Bush et al. [63,74] extended the GW formulation by adopting paraboloidal asperity summits and confirmed the linear scaling of real contact area with load under small deformations. Despite the simplification of neglecting asperity interactions, both the GW and Bush models remain indispensable in tribology, especially for applications involving rubber–road interaction and tire dynamics.

2.3. The Role of Adhesion in Contact Mechanics

Adhesion plays a crucial role in contact mechanics, especially for soft materials such as elastomers [75–78]. Attractive intermolecular forces between solids in close proximity explain why a finite load is needed to separate two bodies in intimate contact [79–81]. This effect is particularly relevant under light loads [24,82]. Experimental studies confirmed that contact areas at low loads are significantly larger than Hertzian predictions and remain finite as the load approaches zero [83,84], consistent with earlier estimates by Bradley [85].

Compared to Hertz, the JKR theory provides a more accurate description of soft materials, as adhesion enlarges the real contact area and thus the friction coefficient, leading to closer agreement with experimental evidence (Figure 5).

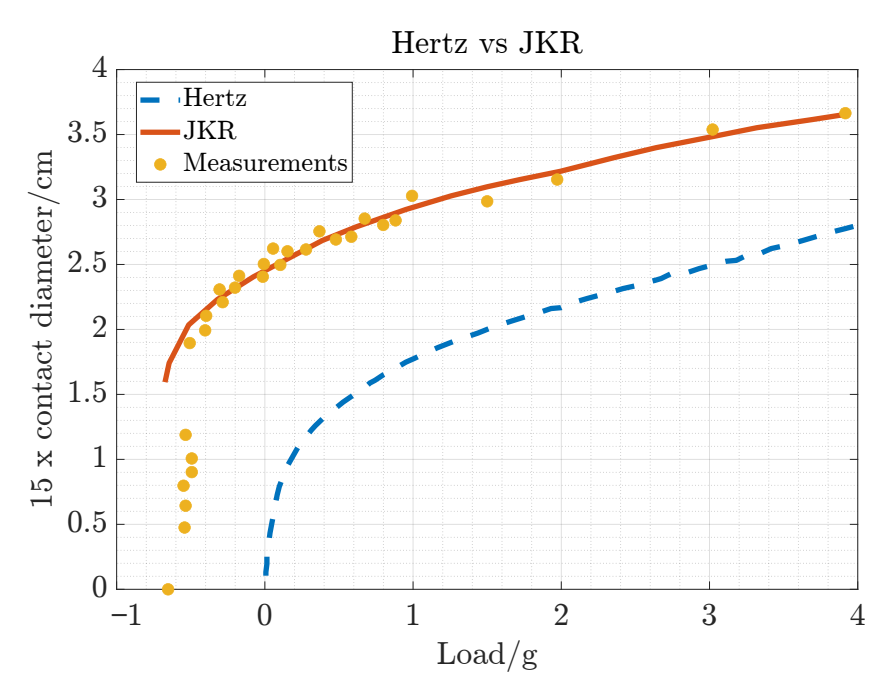


Figure 5. Comparison between JKR and Hertz theory for a rubber sphere in dry contact with a flat surface [86].

Hertzian theory, while foundational, neglects adhesion [33]. Real surfaces, however, experience adhesive interactions at the molecular level that enlarge the contact area beyond purely elastic predictions [25,87,88]. To address this, two classical adhesive contact models were introduced: the Johnson–Kendall–Roberts (JKR) theory [89] and the Derjaguin–Muller–Toporov (DMT) theory [90]. Both extend Hertz's formulation by including van der Waals forces.

The JKR model accounts for adhesion within the contact region, predicting a finite contact radius even at zero load [91–94]. By minimizing the total energy, Johnson et al. derived the contact radius as

$$a^{3} = \frac{3R}{4E^{*}} \left(F + 3\pi R\gamma + \sqrt{6\pi RF\gamma + (3\pi R\gamma)^{2}} \right), \tag{8}$$

where R is the reduced radius of curvature, E^* is the effective elastic modulus (Equation (4)), F is the applied load, and γ is the surface energy. At $\gamma=0$, the Hertz solution is recovered. JKR also predicts a pull-off force:

$$F_{JKR} = \frac{3\pi R\gamma}{2},\tag{9}$$

and a pressure distribution modified by adhesion [89].

Although the original JKR formulation addressed the contact of a sphere on a plane, its methodology is extendable to other geometries, such as sinusoidal surfaces [95].

The DMT theory, in contrast, retains Hertzian stresses inside the contact area but adds adhesive forces acting outside the contact area, modeled via a Lennard–Jones potential [96–99]. Thus, JKR incorporates adhesion inside the contact area, whereas DMT applies it externally. The schematic comparison between JKR and DMT is reported in Figure 6.

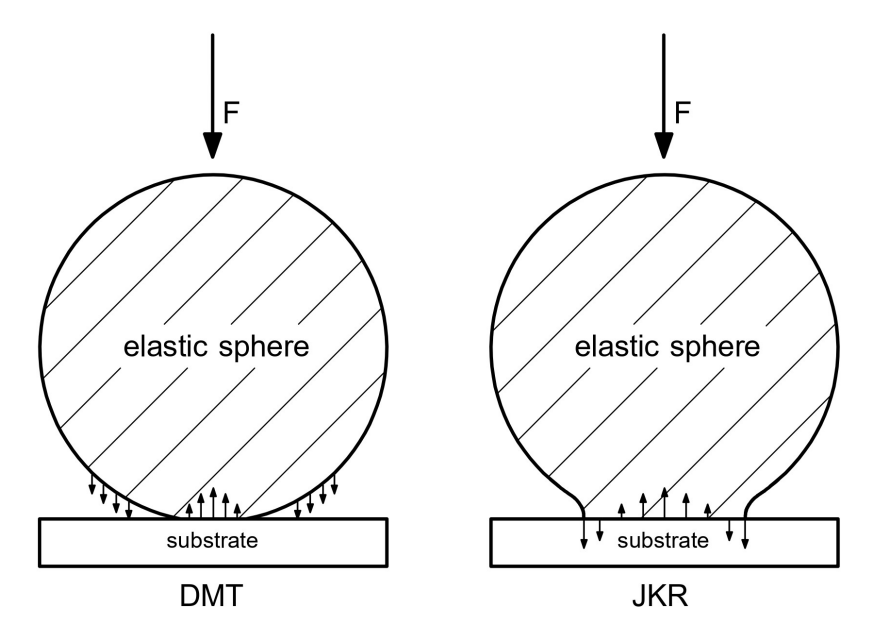


Figure 6. Schematic comparison of the DMT and JKR adhesive contact models [25].

Although conceptually different, both JKR and DMT reduce to the Hertz solution in the absence of adhesion [100]. Initially treated as competing models, their applicability was clarified by Tabor [101], Muller [102] and Maugis [103], who showed that JKR is appropriate for soft, highly adhesive materials, while DMT better describes stiff, weakly adhesive systems [104].

Maugis later introduced a unified formulation [105–108], parameterized by a dimensionless Maugis parameter λ , which quantifies the relative importance of adhesion versus elasticity:

- $\lambda \ll 1$: DMT regime;
- $\lambda \gg 1$: JKR regime.

This parameter corresponds physically to the ratio between adhesion-induced elastic deformation and the range of adhesion forces [109,110].

For typical tire tread compounds, the Maugis parameter λ generally falls within the intermediate transition regime, implying partial adhesion within the contact region. Experimental investigations on filled SBR and NR blends have shown that λ decreases with increasing temperature—mainly due to the reduction in surface energy γ and the elastic stiffening of the rubber matrix. Elevated humidity or hydrophilic surface contamination tends to lower the effective surface energy, shifting the contact behavior toward the DMT limit, whereas clean, dry interfaces reinforced with silica or carbon black exhibit higher λ values. Therefore, real tire—road interactions typically operate in a mixed or transitional regime where both adhesive and elastic contributions coexist.

In summary, adhesive contact models (JKR, DMT, and Maugis' transition theory) demonstrate that adhesion introduces nonlinear relationships between load and contact area, highlighting the limitations of purely elastic theories and the critical role of surface energy in realistic contact mechanics.

2.4. Modern Theories of Contact Mechanics: Rubber Block Sliding on Rough Surfaces

Over the past few decades, significant advances in contact mechanics have been achieved through both experimental tools and numerical simulations [111–114]. A key contribution is the semi-analytical framework of Klüppel and Heinrich, who extended the classical Greenwood and Williamson (GW) model to describe the sliding of rubber on rough surfaces [115,116]. Their approach incorporates the interplay between the viscoelastic

properties of rubber and the multi-scale nature of roughness, accounting for both adhesive and hysteretic friction contributions [117–124].

While the GW theory effectively models hard materials by assuming independent asperities [62], this assumption fails for rubber, where compliant deformation fields overlap at small scales. To address this, Klüppel and Heinrich adapted the GW model to include asperity interactions, thus enabling a more realistic description of the real contact area under sliding with velocity v and vertical load F (Figure 7).

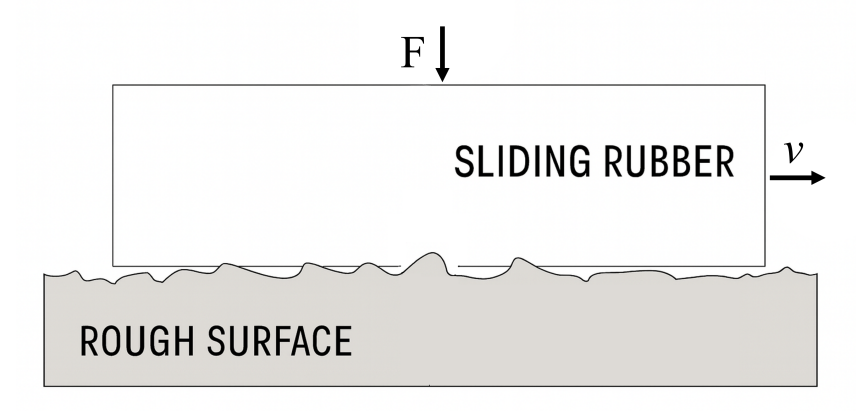


Figure 7. Rubber block sliding with velocity v on a rough counter surface under vertical load F.

In this formulation, the original height distribution $\phi(z)$ is replaced by the summit height distribution $\phi_s(z)$, obtained through an affine transformation, which better describes the portion of the rough profile effectively in contact [116,125]. Introducing the standardized separation $t_s = d/\sigma_s$, the GW functions $F_n(t_s)$ can be evaluated, with $F_0(t_s)$ denoting the probability of summit–rubber contact [115,125].

The model further incorporates the viscoelastic nature of rubber through its dynamic complex modulus $E^*(\omega)$ [126–129]. Under standard assumptions ($\nu_1 = 0.5$, $E_1 \ll E_2$), the effective modulus becomes [125]

$$\frac{1}{E^*} = \frac{1 - \nu_1^2}{E_1} + \frac{1 - \nu_2^2}{E_2} \approx \frac{3}{4|E^*(\omega)|}$$
 (10)

Considering the largest asperities as spherical caps of radius *R*, the normal load and stress can be expressed in terms of the GW functions and the summit height distribution as [115,125,130]

$$F = \frac{16}{9} A_0 N_s |E^*(\xi_{||})| R^{1/2} \sigma_s^{3/2} F_{3/2}(t_s), \tag{11}$$

$$\sigma_0 = \frac{F}{A_0}. (12)$$

Similarly, the macroscopic real contact area $A_{c,0}$ is obtained as a fraction of the nominal area A_0 (Figure 8) and can be related to the fractal dimension D of the surface roughness [115,125,131]:

$$A_{c,0} = \frac{(2D-4)}{12\sqrt{3}(2D-2)} A_0 F_0(t). \tag{13}$$

This fractal characterization is often performed through statistical descriptors such as the Height Difference Correlation (HDC) function [132–134].

Nominal Contact Area Macroscopic Contact Areas

Figure 8. Nominal contact area A_0 and contributions to the macroscopic real contact area $A_{c,0}$.

Because roughness is inherently multi-scale, the real contact area A_c is scale-dependent. The yardstick method [115,135] illustrates this by showing how the apparent contact area increases as smaller cavities are accounted for:

$$A_c(\lambda) = A_{c,0} \left(\frac{\lambda}{\xi_{||}}\right)^{2-D}, \qquad \lambda < \xi_{||}. \tag{14}$$

The smallest scale at which rubber conforms, λ_{min} , is determined by an energy balance between deformation, adhesion, and stored elastic energy [115]. This defines the effective real contact area $A_c(\lambda_{min})$, which is generally below 10% of the nominal contact area A_0 at high velocities and low loads [116].

In practical numerical implementations, λ_{\min} is obtained by numerically solving the energy-balance condition for the unknown wavelength under the assigned operating conditions (velocity, contact pressure, and temperature). The computation uses the viscoelastic modulus $E^*(\omega)$ —evaluated at $\omega = 2\pi v/\lambda$ via time–temperature superposition—and the surface spectral descriptors as inputs. Hence, λ_{\min} represents the smallest wavelength at which the deformation energy of rubber still compensates for the combined elastic and adhesive contributions.

Recognizing that road surfaces are better described by two scaling regimes (macroand micro-texture), Klüppel and Heinrich extended their theory accordingly [115,125]. The contact area expression then becomes

$$A_c(\lambda) = A_{c,0} \left(\frac{\lambda_2}{\xi_{||}}\right)^{2-D_1} \left(\frac{\lambda_{min}}{\lambda_2}\right)^{2-D_2}.$$
 (15)

The adoption of two scaling regimes is not arbitrary but reflects the two distinct slopes typically observed in asphalt spectra (macro- vs. micro-texture).

Some results from this theory, showing the ratio A_c/A_0 as a function of sliding velocity and pressure, are reported in Figure 9. Increasing velocity reduces A_c as rubber becomes glassy, while higher contact pressure increases indentation depth and enlarges the real area of contact. Overall, A_c remains a small fraction of A_0 .

In summary, the Klüppel–Heinrich extension of the GW framework captures the scale-dependent behavior of rubber sliding on rough surfaces by combining fractal descriptors of roughness with the viscoelastic properties of elastomers. This provides a solid physical basis for the subsequent development of tire friction models.

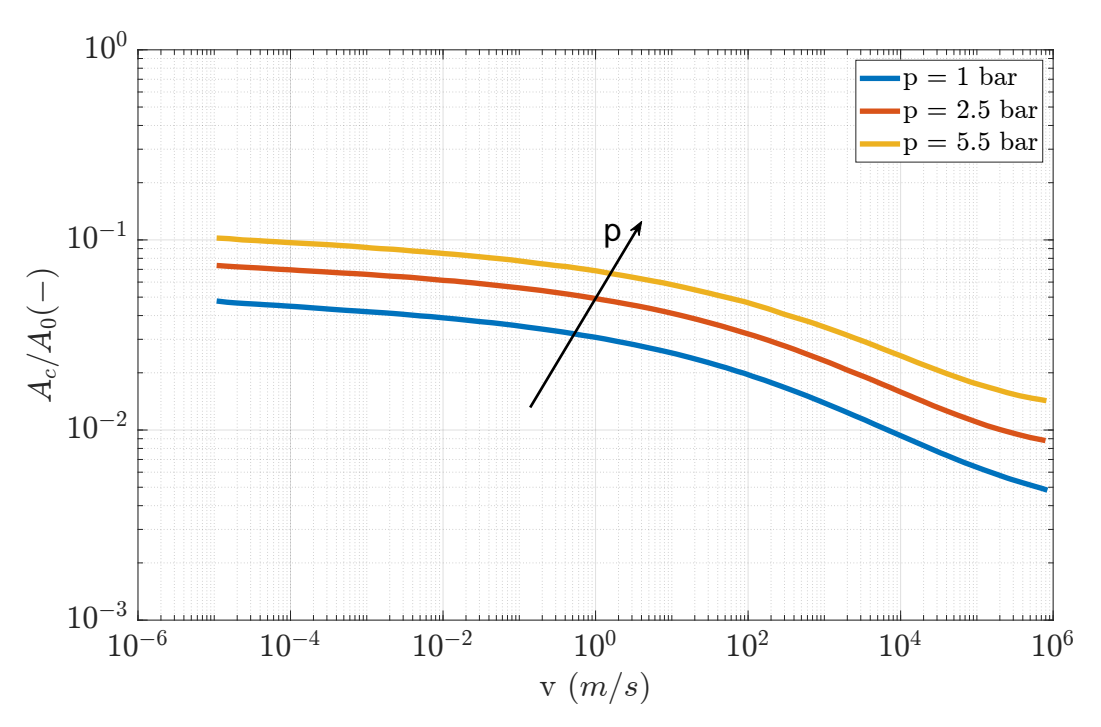


Figure 9. Ratio of real to nominal contact area as a function of sliding velocity at different pressures, with model results following Klüppel–Heinrich prediction computed and plotted by the authors [116].

While Klüppel and Heinrich's framework provides a physically grounded extension of GW to viscoelastic rubber on multiscale roughness, several assumptions (e.g., discrete asperities, limited coupling across scales) motivate alternative descriptions. Persson's theory instead treats surface roughness as a continuous random field and formulates contact as a scale-evolving stochastic process in stress space, offering a complementary and often more general perspective on rubber–road interactions [136–141].

In Persson's approach, the interface is examined at increasing magnifications $\zeta = L/\lambda$, where L is the macroscopic contact diameter and λ is the smallest resolved length scale [76, 142]. As ζ increases, new roughness wavelengths become visible and previously apparent contact regions are revealed as (partly) non-contact regions. The relative contact area at magnification ζ is

$$P(\zeta) = \frac{A(\zeta)}{A_0}, \quad \text{with } \sigma_0 A_0 = \langle \sigma \rangle_{\zeta} A(\zeta),$$
 (16)

so that $P(\zeta) = \sigma_0 / \langle \sigma \rangle_{\zeta}$. The average local pressure $\langle \sigma \rangle_{\zeta}$ follows from the stress probability density $P(\sigma, \zeta)$:

$$\langle \sigma \rangle_{\zeta} = \frac{\int_{0}^{\infty} \sigma P(\sigma, \zeta) \, d\sigma}{\int_{0}^{\infty} P(\sigma, \zeta) \, d\sigma}.$$
 (17)

The evolution of $P(\sigma, \zeta)$ is governed by a diffusion-like equation in which "time" is replaced by magnification [142]:

$$\frac{\partial P(\sigma,\zeta)}{\partial \zeta} = f(\zeta) \frac{\partial^2 P(\sigma,\zeta)}{\partial \sigma^2},\tag{18}$$

supplemented by (i) a reflecting/absorbing boundary at zero tension in the non-adhesive case [143], $P(0,\zeta)=0$, and (ii) the initial condition $P(\sigma,\zeta=1)=\delta(\sigma-\sigma_0)$, i.e., uniform macroscopic pressure σ_0 . The diffusion coefficient couples elasticity and roughness via the power spectral density (PSD) C(q):

$$f(\zeta) = \frac{\pi}{4} \left(\frac{E}{1 - \nu^2} \right)^2 q(\zeta)^2 C(q(\zeta)), \qquad q(\zeta) = q_L \zeta, \ q_L = \frac{2\pi}{L}, \tag{19}$$

where *E* is the effective modulus and ν is the Poisson ratio [142,144].

Solving (18) yields the contact fraction at scale *q*:

$$P(q) = \frac{2}{\pi} \int_0^\infty \frac{\sin x}{x} \exp\left[-x^2 G(q)\right] dx, \tag{20}$$

with the cumulative roughness-rheology functional

$$G(q) = \frac{1}{8} \int_{q_L}^{q} q'^3 C(q') \int_0^{2\pi} \left| \frac{E(q'v\cos\phi)}{(1-v^2)\sigma_0} \right|^2 d\phi \ dq', \tag{21}$$

where $E(\omega)$ is the complex (frequency-dependent) modulus evaluated at $\omega = q'v\cos\phi$, with v being the sliding speed and ϕ being the angle between \vec{q} and the sliding direction [142].

For $\sigma_0 \ll |E(\omega)|$, the small-*x* limit of (20) gives the widely used approximation

$$P(q) \simeq \left[\pi G(q)\right]^{-1/2},\tag{22}$$

and an accurate interpolation valid across regimes is [142]

$$P(q) \approx \left(1 + \left[\pi G(q)\right]^{3/2}\right)^{-2/3}.$$
 (23)

The real contact area at the finest resolved scale q_1 is therefore

$$A_c = A_0 P(q_1), (24)$$

with lower and upper cutoffs (q_0, q_1) bounding the self-affine PSD (macro to micro/atomic scales). In practice, q_1 reflects physical limitations (contamination layers, surface films, molecular smoothing), ensuring a finite A_c even if the mathematical self-affinity extends to very high q [142].

Persson proposed an empirical rule for q_1 based on the rms slope of the surface:

$$h_{\rm rms}^2 = \frac{1}{2\pi} \int_{q_0}^{q_1} C_{2D}(q) \, dq \approx 1.3,$$
 (25)

which fixes the upper cutoff by imposing a target slope level [111,145]. The upper cutoff is thus defined following Persson's slope-weighted description of roughness, which properly accounts for short-wavelength features rather than relying solely on height amplitudes; this prevents bias in the real contact area estimate by correctly weighting spatial frequencies.

While convenient, this method does not capture potential changes in rubber behavior and chemistry at very small scales [146,147], and, more broadly, the choice of (λ_0, λ_1) (or (q_0, q_1)) remains debated due to the lack of predictive mechano-chemical models for surface evolution under local stress/temperature.

Unlike asperity-based models, Persson's theory (i) directly embeds the multiscale PSD into the contact solution, (ii) naturally incorporates viscoelastic dispersion via $E(\omega)$ at each q-scale, and (iii) predicts that P decreases with increasing magnification, while friction can remain finite because energy dissipation accumulates across scales [136,137,139]. This statistical mechanics view has become a cornerstone for modern friction modeling and will underpin later developments discussed in the next section.

Beyond Persson, recent work by Müser and co-authors has analyzed nonlinearity and nonlocality in soft–hard contact, elucidating how microscale morphology and long-range elastic coupling regulate contact area and interfacial forces [148,149].

3. Fundamentals of Friction Theories

While contact mechanics establishes a framework for stresses and deformations at interfaces, friction theories extend this foundation to explain how these interactions translate into energy dissipation and grip. Rubber friction is a complex phenomenon influenced by road roughness, contact area geometry, compound viscoelasticity, sliding velocity, and interface temperature. Since the forces exchanged between the tire and road are fundamentally frictional, understanding these mechanisms is crucial for tire performance analysis [150]. Over time, numerous theories have been developed to describe tire—road interaction [151–153]. The effective friction coefficient is generally attributed to three contributions: hysteresis, adhesion, and wear [154,155].

The hysteresis component (or indentation friction) originates from the internal viscoelastic deformation induced by asperities. As rubber slides, the time-dependent response generates asymmetric pressure fields that oppose motion [156–159].

The adhesive component arises from molecular interactions (e.g., van der Waals forces) forming at the true contact spots [160–166]. During sliding, bonds form, stretch and break, with viscoelastic resistance contributing to friction. At higher sliding velocities, reduced bonding time lowers the adhesive contribution [25,167,168]. Adhesion also increases the effective area involved in hysteretic losses [154].

The third contribution, wear-related friction, occurs when sharp asperities excite the rubber at high frequencies, possibly inducing local microfractures and energy dissipation [169]. However, this effect is usually negligible compared to adhesion and hysteresis and was already considered minor in practical conditions by the 1960s [154].

Based on these considerations, the total friction force F is expressed as [154]

$$F = F_a + F_h \tag{26}$$

where F_a and F_h are the adhesive and hysteretic contributions, respectively. A schematic illustration of these mechanisms is shown in Figure 10.

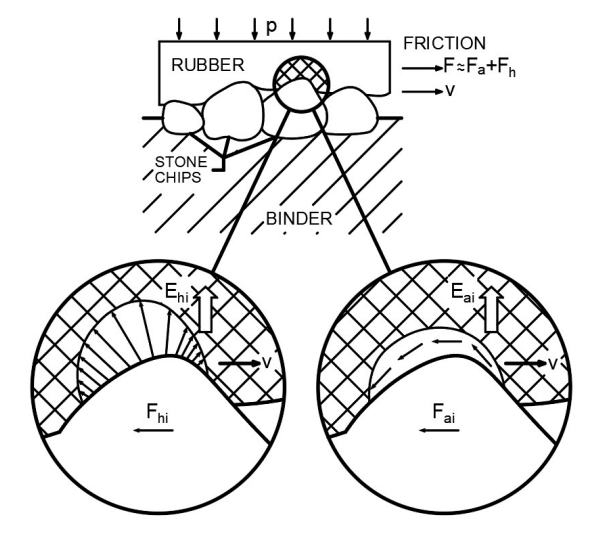


Figure 10. Friction forces developed during tire–road interaction [155].

By dividing Equation (26) by the normal load, one obtains the total friction coefficient:

$$\mu = \mu_a + \mu_h \tag{27}$$

where μ_a and μ_h denote the adhesive and hysteretic components. In wet conditions, the adhesive term is strongly reduced by the water film, so most of the grip arises from hysteresis.

Experimentally, the two mechanisms can be separated by repeating friction tests on the same rubber/roughness pair with and without a thin inert lubricant (or dusting), which strongly suppresses interfacial shear while leaving bulk viscoelastic hysteresis essentially unaffected, so that the difference estimates the adhesive share. Although such procedures cannot fully remove adhesion, they provide a practical means to quantify its relative contribution. From a computational standpoint, adhesion is mainly associated with the low-frequency range corresponding to slow interfacial slip, whereas hysteresis dominates the higher frequencies linked to bulk viscoelastic deformation. These distinct spectral domains—interfacial for adhesion and bulk for hysteresis—naturally prevent double counting when the two mechanisms are superposed in hybrid models.

Over the years, several experimental and theoretical contributions have advanced the understanding of these mechanisms, as will be discussed in the following sections.

3.1. Grosch's Experimental Tests

One of the pioneers in rubber friction studies was Grosch, who conducted systematic experiments to identify the main mechanisms of friction [170–173]. He showed that rubber friction is primarily governed by adhesion and hysteresis and related these contributions to the viscoelastic properties of rubber compounds.

Grosch tested four rubbers (INR, ABR, SBR, butyl) against smooth glass and rough silicon carbide. Friction was measured using a rig where the sample was pressed against the surface under controlled temperature ($-50\,^{\circ}\text{C}$ to $100\,^{\circ}\text{C}$) and humidity, with sliding velocities up to 30 mm/s to avoid heating effects. The data were shifted into master curves using the Williams–Landel–Ferry (WLF) equation [174–176].

For SBR and ABR, two distinct peaks appeared in the master curves: a low-velocity peak associated with adhesion and a high-velocity peak attributed to hysteresis. Suppressing molecular contact by dusting the surface reduced only the first peak, confirming this interpretation.

Two characteristic length scales emerged from these results. For adhesion, Grosch found a constant ratio between the velocity at the first peak and the frequency of maximum loss modulus, corresponding to a molecular slip distance of about 6×10^{-9} m. For hysteresis, the velocity of the second peak was related to the frequency of maximum loss tangent, corresponding to a length scale of 1.5×10^{-4} m, consistent with the average asperity spacing.

These characteristic lengths should not be regarded as universal constants but as empirical correlations arising from the interplay between the viscoelastic spectrum of the compound and the surface morphology. Their magnitude can vary with filler morphology, crosslink density, temperature, and surface cleanliness, yet their order of magnitude remains consistent across typical tire rubbers and test surfaces, supporting Grosch's mechanistic interpretation of adhesive and hysteretic friction processes.

These scales reflect the essence of the two mechanisms: adhesion dominates at the molecular level when the rubber enters the glassy regime, while hysteresis peaks in the rubbery–glassy transition region, where internal viscoelastic losses are maximized.

Grosch's work thus provided the first clear experimental separation of adhesive and hysteretic contributions, and his master curves remain a cornerstone for later theories describing friction on multiscale rough surfaces, including those of Klüppel–Heinrich [114,116] and Persson [142,145].

3.2. Klüppel and Heinrich's Friction Model

The model developed by Klüppel and Heinrich is based on the fractal scaling of rough surfaces and the linear viscoelastic response of rubber [115,116,125]. It considers both

hysteresis and adhesion contributions during sliding, with explicit treatment of micro- and macro-scale roughness.

The hysteresis component is obtained by evaluating the energy dissipated through viscoelastic deformation over a spectrum of excitation frequencies activated during sliding [116]:

$$\mu_{hys}(v) = \frac{F_{hys}}{F_N} = \frac{\langle \delta \rangle}{2\sigma_0 v} \int_{\omega_{min}}^{\omega_{max}} \omega E''(\omega) S(\omega) d\omega, \tag{28}$$

where E'' is the loss modulus, $S(\omega)$ is the power spectral density of the surface, σ_0 is the nominal stress, and $\langle \delta \rangle$ is the mean thickness of the deformed layer. The latter is proportional to the penetration depth $\langle z_p \rangle$, itself related to nominal stress by Hertzian arguments [62,125,177]:

$$\langle \delta \rangle = b \langle z_p \rangle, \qquad \langle z_p \rangle = \frac{\pi \xi_{\parallel}}{E'(\omega_{min})} \sigma_0,$$
 (29)

where b is a scaling parameter depending on strain level (Figure 11) [178].

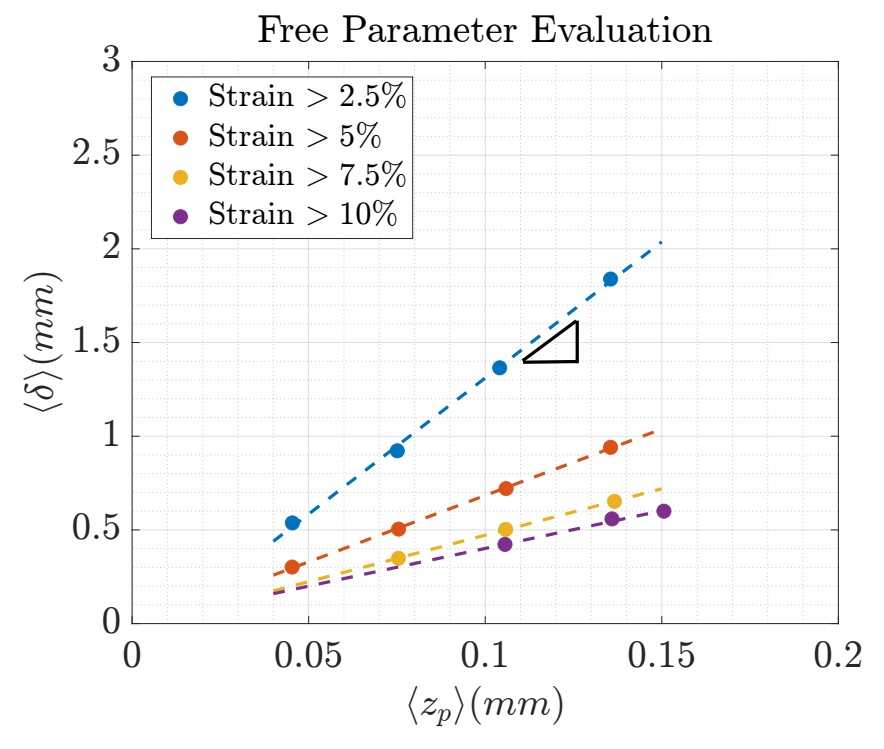


Figure 11. Fitted parameter *b*, computed and plotted by the authors (see [178]).

Thus, b is obtained from the slope of the linear fit between $\langle \delta \rangle$ and $\langle z_p \rangle$ at different strain levels, as shown in Figure 11.

For surfaces with two fractal scaling regimes, the integral is split into macro and micro ranges [115,125]:

$$\mu_{hys}(v) = \frac{\langle \delta \rangle}{2\sigma_0 v} \left(\int_{\omega_{min}}^{\omega_x} \omega E''(\omega) S(\omega) \, d\omega + \int_{\omega_x}^{\omega_{max}} \omega E''(\omega) S(\omega) \, d\omega \right). \tag{30}$$

At high velocities, the micro-range contribution vanishes as λ_{min} grows, and only macro-roughness remains effective.

The adhesive part is modeled as [114,115]:

$$\mu_{adh}(v) = \frac{F_{adh}}{F_N} = \frac{\tau_s(v)}{\sigma_0} \frac{A_c(v, T, \sigma_0)}{A_0},$$
(31)

where A_c/A_0 is the real-to-nominal contact area ratio (see Section 2.4) and $\tau_s(v)$ is the velocity-dependent interfacial shear stress:

$$\tau_s(v) = \tau_{s_0} \left(1 + \frac{E_{\infty}/E_0}{\left(1 + \frac{v_c}{v} \right)^n} \right),$$
(32)

where $\tau_{s_0} = \gamma_{rs}/l_s$, E_{∞}/E_0 is the glassy-to-rubbery modulus ratio, n is linked to the relaxation spectrum exponent m by n = (1-m)/(2-m) [179], and v_c is a critical velocity depending on T_g and filler content. Persson's theory suggests that $v_c \approx v_0 (E_{\infty}/E_0)^3$, with $v_0 = a_0/(2\pi\tau_0)$ [115], where τ_0 is the entanglement time.

Representative results show that the model reproduces the decrease in dry friction with increasing load, independently of velocity and temperature (Figure 12) [116].

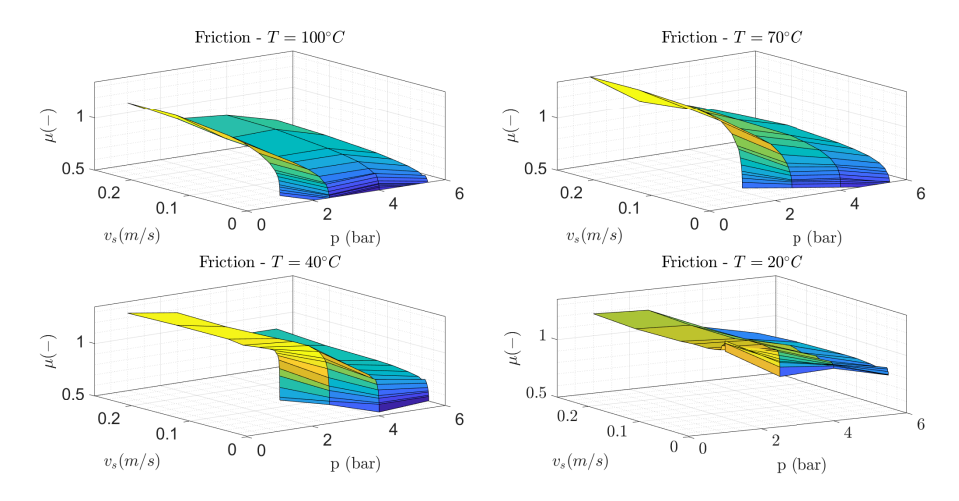


Figure 12. Dry friction coefficients on coarse granite vs. sliding velocity for different pressures and temperatures; model from [116], replotted by the authors.

In summary, Klüppel and Heinrich's model provides a physically grounded description of dry rubber friction by combining fractal surface statistics, viscoelastic dissipation, and interfacial adhesion. It successfully captures the load and velocity dependence of measured friction, laying the basis for comparison with alternative formulations.

3.3. Persson's Friction Model

Persson developed a multiscale theory that links the friction coefficient to sliding velocity by integrating viscoelastic energy dissipation over the full roughness spectrum [142]. Unlike the Klüppel–Heinrich model, it uses the 2D power spectral density (PSD) of surface roughness as input, thus characterizing the interface in a fully three-dimensional manner. A key ingredient is the real contact area, introduced in Section 2.4.

In sliding, the surface displacement field u_i at z = 0 is defined via elastodynamics:

$$u_i(q,\omega) = \frac{1}{(2\pi)^3} \int d^2x \, dt \, u_i(x,t) \, e^{-i(qx-\omega t)},$$
 (33)

and the hysteresis contribution follows from the fluctuating traction produced by asperities [142]:

$$\mu_{hys} = \frac{1}{2} \int_{q_0}^{q_1} q^3 C(q) P(q) \int_0^{2\pi} \cos \phi \operatorname{Im} \left[\frac{E^*(qv \cos \phi)}{(1 - v^2)\sigma_0} \right] d\phi \, dq, \tag{34}$$

where C(q) is the (2D) PSD, E^* is the complex modulus, σ_0 is the nominal pressure, v is the sliding velocity, and ϕ is the angle between q and the sliding direction.

Incomplete contact is captured by

$$P(q) = \frac{1}{\sqrt{\pi}} \int_0^{\sqrt{G(q)}} e^{-x^2/4} dx = \text{erf}\left(\frac{1}{2\sqrt{G(q)}}\right), \tag{35}$$

with

$$G(q) = \frac{1}{8} \int_{q_0}^{q_1} q^3 C(q) \int_0^{2\pi} \left| \frac{E^*(qv\cos\phi)}{(1-v^2)\sigma_0} \right|^2 d\phi \, dq. \tag{36}$$

Water or contaminants can be incorporated by reducing the upper cutoff q_1 (filled cavities), which lowers predicted friction [142].

A central sensitivity of the model is the choice of q_1 (or magnification ζ_{max}): including finer scales increases friction [180].

Persson later included flash temperature effects, which modify E^* through time-temperature superposition (e.g., WLF) when $v \gtrsim 10^{-2}$ m/s [174,181–184]. The temperature field T(x,t) in the rubber satisfies

$$\frac{\partial T}{\partial t} - D_T \nabla^2 T = \frac{\dot{Q}(x, t)}{\rho C_V},\tag{37}$$

leading to a scale-dependent flash temperature T_q (computed iteratively). In practice, the scale-dependent flash temperature T_q is obtained by updating the local viscoelastic modulus $E^*(\omega, T_q)$ through time–temperature superposition until the temperature increment between iterations falls below a small threshold (typically 1–2%), without significant computational overhead for single-point evaluations. The resulting non-isothermal generalizations of (34) and (36) are

$$\mu_{hys} = \frac{1}{2} \int_{q_0}^{q_1} q^3 C(q) P(q) \int_0^{2\pi} \cos \phi \, \text{Im} \left[\frac{E^*(qv \cos \phi, T_q)}{(1 - v^2)\sigma_0} \right] d\phi \, dq, \tag{38}$$

$$G(q) = \frac{1}{8} \int_{q_0}^{q_1} q^3 C(q) \int_0^{2\pi} \left| \frac{E^*(qv\cos\phi, T_q)}{(1 - v^2)\sigma_0} \right|^2 d\phi \, dq.$$
 (39)

Physically, at intermediate magnifications (roughly $\zeta \sim 2-5$), the interface consists of spaced macro-asperity contacts that heat rapidly; at higher magnifications, dense micro-asperities within each macro-contact area interact thermally and elastically, requiring the multi-scale averaging used for T_q [181].

Persson initially neglected adhesion for typical lower cutoffs (\gtrsim 0.1 μ m) [142]. However, subsequent studies have attempted to investigate the adhesive contribution more thoroughly, although this aspect of friction remains largely empirical and not well understood [185], and he later proposed an empirical adhesive term similar to Klüppel's [186]:

$$\mu_{adh} = \frac{\tau_f}{p_0} \frac{A_c}{A_0}, \qquad \tau_f = \tau_{f_0} \exp \left[-c \left(\log_{10} \frac{v}{v_c} \right)^2 \right], \tag{40}$$

where τ_{f_0} is typically 5–11 MPa, $c \approx 0.1$, and v_c is thermally activated:

$$v_c = v_0 \exp \left[-\frac{\epsilon}{k_B} \left(\frac{1}{T} - \frac{1}{T_g} \right) \right], \tag{41}$$

where $v_0 = v_0^* \exp[(\epsilon/k_B)(T_0^{-1} - T_{g_0}^{-1})] \approx 5 \times 10^{-7} \,\text{m/s}$ (definitions as in the original formulation).

Several studies have revisited or leveraged Persson's framework. Ciavarella proposed simplified formulations starting from the cutoff selection problem [146,187].

Fina et al. compared Grosch's data [170] with Persson's predictions: after tuning material parameters (but not q_1), the hysteresis peak was captured while low-/high-speed discrepancies persisted, likely due to missing adhesion and spectral differences [188].

More recently, Furlan and Mavros used an ANN to replicate Persson's flash temperature friction model, enabling real-time friction estimation from compound operating conditions and surface spectra. Integrated into a tire and vehicle model, it captured surface-dependent variations with notable effects on braking and handling. [189].

Overall, Persson's theory provides a rigorous multiscale connection between PSD, viscoelasticity, and operating conditions, and—since being extended to flash temperature—it has become a cornerstone for both fundamental studies and applied tire models. Its main limitations are the sensitivity to the upper cutoff (magnification) [180] and the computational cost of the non-isothermal implementation, which motivate ongoing simplifications and hybrid approaches.

4. Discussion and Research Gaps

The preceding sections reviewed the main theories describing rubber contact with rough surfaces and the resulting friction. Despite differences in complexity and assumptions, all models address how surface roughness, viscoelastic behavior, and operating conditions influence real contact area and energy dissipation. This concluding section compares the models, outlines their strengths and limitations, and identifies open research gaps.

4.1. Critical Analysis of Contact Mechanics Models

Classical approaches to contact mechanics, such as Hertzian theory, provide the analytical foundation for contact analysis but are inadequate when applied to elastomers in contact with rough surfaces. Hertz assumes smooth, perfectly elastic bodies and therefore neglects the multiscale roughness, viscoelasticity, and adhesion typical of rubber interfaces. Despite these limitations, it remains a useful baseline for comparison.

The Greenwood–Williamson (GW) model improved upon Hertz's model by introducing a statistical description of surface roughness through an ensemble of asperities. This allowed for partial contact and roughness distributions to be considered, but simplifications such as identical spherical asperities, uncorrelated heights, and purely elastic interactions limit its applicability to rubber, especially as it omits frequency-dependent viscoelastic effects and scale transitions.

Adhesive contact theories, particularly the Johnson–Kendall–Roberts (JKR) formulation, extended Hertz by including adhesion at the contact edge. JKR is relevant for compliant systems and small scales but still assumes smooth geometries and does not incorporate roughness or viscoelastic effects. Nevertheless, it established the basis for more advanced adhesive contact models.

Modern multiscale approaches addressed these shortcomings by combining fractal surface descriptions with viscoelastic rheology. Klüppel and Heinrich introduced a framework in which an energy-based condition defines the minimum contact length scale, below which contact becomes negligible. This concept links roughness geometry and frequency-dependent rubber response, offering a more realistic picture of load support and dissipation across scales.

Persson's theory further advanced this view by analyzing contact as a function of magnification, using the surface power spectral density (PSD) instead of discrete asperities. Large-scale features dominate at low magnification, while finer scales emerge as magnification increases. The introduction of the cutoff wavevector q_1 defines the finest roughness scale included, but the absence of a universally accepted criterion for its selection makes predictions highly sensitive to this choice.

Overall, while modern multiscale models offer more realistic descriptions of rough contact, they face challenges related to parameter identification, sensitivity to PSD cutoffs, and computational demands. Both Klüppel–Heinrich and Persson provide strategies for scale separation and contact area estimation, but with different assumptions and mathematical treatments. Comparative analysis of their predictions remains an open research topic.

Table 1 summarizes the main contact mechanics models, highlighting their respective strengths and limitations.

Table 1. Comparison of contact models.

Models	Strengths	Limitations
Hertz	Simple and analytically solvable Applicable for smooth, elastic bodies Closed-form solutions for stress, deformation and contact radius	Assumes idealized smooth surfaces Ignores roughness and adhesion Limited to small elastic deformations
JKR	Incorporates adhesion into contact analysis Relevant for soft materials and micro/nanoscale contacts Extends Hertz to include surface energy effects	Assumes perfectly smooth surfaces Limited for rough or multiscale contacts Strong dependence on surface energy estimates
Greenwood-Williamson	Introduces statistical roughness description Estimates contact area and pressure via asperity height distributions	Assumes identical, spherical, non-interacting asperities Neglects elastic coupling and scale dependence
Klüppel and Heinrich	Includes viscoelastic effects and scaling Defines minimum contact length and real contact evolution	Requires empirical cutoff parameters Relies on simplified statistical descriptors
Persson	Fully multiscale, PSD-based formulation Accounts for roughness and viscoelasticity across scales	Mathematically complex Sensitive to cutoff wavevectors and magnification

4.2. Comparative Discussion of Friction Models

Friction modeling has evolved from empirical observations to increasingly sophisticated multiscale theories. Grosch's pioneering experiments [170] established the correlation between the coefficient of friction and the viscoelastic response of rubber, showing how sliding velocity and temperature govern energy dissipation. These insights laid the foundation for hysteresis-based models, highlighting the frequency dependence of friction.

Building on this, Klüppel and Heinrich [115,116] developed a semi-analytical framework that decomposes roughness into micro- and macro-asperity contributions. Their model extends Greenwood–Williamson contact mechanics to rubber sliding, integrates the power-law behavior of viscoelastic dissipation, and introduces a dynamic interaction function linking excitation frequencies to friction. While effective in reproducing the bell-shaped μ –v curve, the model requires calibration through fitting parameters and treats adhesion in an empirical way.

Persson's model [142,181] provides a more unified formulation by explicitly coupling his multiscale contact theory with energy dissipation. By incorporating the 2D power spectral density (PSD) of surfaces, it treats roughness in three dimensions and naturally accounts for scale-dependent viscoelastic losses. The later extension to flash temperature explains the friction decay at high velocities, although at the cost of significant computational effort. Adhesion was subsequently introduced in Persson's framework, but still through empirical assumptions that limit predictive robustness.

To address computational challenges, Furlan and Mavros [189] trained artificial neural networks (ANNs) to emulate Persson's flash temperature model. Their implementation demonstrated real-time capability, making integration into tire and vehicle simulations feasible. However, the ANN approach sacrifices interpretability, relying instead on data-driven replication of the original physics-based model.

A comparative summary of the main friction models is presented in Table 2.

Table 2.	Comp	oarison	of fr	riction	theories.

Models	Strengths	Limitations
Grosch Tests (1963)	First to demonstrate μ –frequency dependence Linked friction to viscoelastic modulus peaks Provided basis for later theoretical models	Purely empirical: no predictive capability Cannot compute μ from compound or surface parameters
Klüppel and Heinrich	Semi-analytical, multiscale approach Evaluates hysteresis and adhesion contributions Incorporates cutoff length and viscoelastic losses	Adhesion modeled empirically Requires parameter fitting No flash temperature treatment
Persson	Fully multiscale framework using PSD Directly links friction to viscoelastic moduli Includes flash temperature effects	Computationally expensive Sensitive to cutoff wavevector Adhesion term remains empirical

Beyond conceptual differences, quantitative comparison among the reviewed models can be achieved by expressing results in terms of directly measurable quantities. In practice, the key quantities—surface power spectral density, viscoelastic moduli and cutoff wavevectors—can be obtained from surface texture (via profilometric measurements) analysis and dynamic mechanical analysis, enabling reproducible benchmarking across compounds and roughness scales. Recent progress in surface metrology, high-speed thermography, and finite-element or reduced-order simulations provides the computational tools necessary to implement these models in predictive workflows, thus facilitating their adoption by engineers and practitioners.

Under equivalent operating conditions, both frameworks predict similar qualitative trends but differ quantitatively in their sensitivity to input parameters. The Klüppel–Heinrich model, being based on discrete asperity statistics, shows a clear dependence of the A_c/A_0 on the applied pressure and a monotonic reduction with increasing sliding velocity due to the glass transition of the compound. Persson's theory, in contrast, exhibits a stronger dependence on the upper cutoff q_1 and captures nonlinear reductions of A_c/A_0

with magnification, leading to slightly lower friction levels at high velocities when flash temperature effects are included.

4.3. Research Gaps and Future Challenges

Despite significant progress, several open challenges remain in the contact and friction modeling of rubber. A central issue is the definition of cutoff criteria: most advanced models depend on a cutoff wavevector or length scale, yet its selection is often empirical and strongly affects predictions. Related to this, thermo-mechanical coupling across scales and its impact on contact area and friction remain only partially understood.

Adhesion is another unresolved aspect. While minor at high speeds and loads, it dominates at low loads or in clean, dry conditions. Current models (e.g., Klüppel and Persson) treat adhesion empirically, and a rigorous, experimentally validated adhesive formulation is still lacking. Similarly, the representation of surface roughness through power spectral density (PSD) is limited by measurement resolution and data truncation, raising the need for complementary descriptors to fully characterize road textures.

Computational tractability is also a key limitation. Persson's flash temperature model, for example, is too demanding for large-scale or real-time applications, while surrogate models improve efficiency at the cost of physical interpretability. Furthermore, most models are calibrated on restricted conditions (e.g., sandpaper, single compounds, narrow velocity ranges), limiting generalization to realistic surfaces, multiple compounds, or variable environments. The absence of extensive experimental benchmarks hampers validation.

Future developments should aim to achieve a more quantitative and physically grounded understanding of adhesion under realistic tire—road conditions. This will likely require in situ diagnostics capable of capturing interfacial temperature, stress, and detachment dynamics, together with multiscale models that incorporate such data in a physically consistent way. Coupling experimental evidence with data-driven techniques may ultimately provide a pathway toward predictive adhesive friction. Nevertheless, it should be emphasized that the quantification of the adhesive contribution remains a topic of active debate within the tribology community and is still far less understood than the hysteretic counterpart.

In summary, current theories—from classical contact to multiscale viscoelastic frameworks—have greatly advanced the understanding of tire—road interaction. Yet, major research gaps persist regarding multiscale coupling, adhesion, roughness representation, and computational efficiency. Future progress will depend on integrating high-resolution experimental methods, improved surface characterization, hybrid physics—data-driven approaches, and validation within full vehicle simulations, thus bridging the gap between academic insight and industrial applicability.

Author Contributions: Conceptualization, R.S.; Methodology, R.S. and G.F.; Formal Analysis, R.S. and A.G.; Investigation, R.S., G.N.D. and A.S.; Resources, R.S., G.N.D. and A.S.; Data Curation, R.S. and G.F.; Writing—original draft preparation, R.S.; writing—review and editing, G.F. and F.F.; Visualization, R.S., G.F. and A.G.; Supervision, A.S., F.T. and F.F.; Project Administration, F.T. and F.F. All authors have read and agreed to the published version of the manuscript.

Funding: This work was partly supported by the project "FINGERTIPS—Friction-Increase Nanopoles and Grooves Exploitation in Road-Tire Interaction for Preventive Safety" funded by the Italian MUR "Progetti di Ricerca di Rilevante Interesse Nazionale (PRIN 2022 PNRR PE8)"—grant n. P2022LZWF5—P.I. Flavio Farroni.

Institutional Review Board Statement: Not applicable.

Informed Consent Statement: Not applicable.

Data Availability Statement: Not applicable.

Conflicts of Interest: The authors declare no conflicts of interest.

References

- Johnson, K.L.; Johnson, K.L. Contact Mechanics; Cambridge University Press: Cambridge, UK, 1987.
- 2. Alvarez, L.; Yi, J.; Horowitz, R.; Olmos, L. Dynamic friction model-based tire-road friction estimation and emergency braking control. *J. Dyn. Sys. Meas. Control* **2005**, 127, 22–32. [CrossRef]
- 3. Barber, J.R.; Ciavarella, M. Contact mechanics. Int. J. Solids Struct. 2000, 37, 29–43. [CrossRef]
- 4. van Kuilenburg, J.; Masen, M.A.; van der Heide, E. A review of fingerpad contact mechanics and friction and how this affects tactile perception. *Proc. Inst. Mech. Eng. Part J J. Eng. Tribol.* **2015**, 229, 243–258. [CrossRef]
- 5. Barbaro, M.; Genovese, A.; Timpone, F.; Sakhnevych, A. Extension of the multiphysical magic formula tire model for ride comfort applications. *Nonlinear Dyn.* **2024**, *112*, 4183–4208. [CrossRef]
- 6. Dutkiewicz, M.; Velychkovych, A.; Shatskyi, I.; Shopa, V. Efficient model of the interaction of elastomeric filler with an open shell and a chrome-plated shaft in a dry friction damper. *Materials* **2022**, *15*, 4671. [CrossRef]
- 7. Shatskyi, I.; Velychkovych, A. Analytical model of structural damping in friction module of shell shock absorber connected to spring. *Shock Vib.* **2023**, 2023, 4140583. [CrossRef]
- 8. Velychkovych, A.; Mykhailiuk, V.; Andrusyak, A. Numerical model for studying the properties of a new friction damper developed based on the shell with a helical cut. *Appl. Mech.* **2025**, *6*, 1. [CrossRef]
- 9. Velychkovych, A.; Mykhailiuk, V.; Andrusyak, A. Evaluation of the Adaptive Behavior of a Shell-Type Elastic Element of a Drilling Shock Absorber with Increasing External Load Amplitude. *Vibration* **2025**, *8*, 60. [CrossRef]
- 10. Shull, K.R. Contact mechanics and the adhesion of soft solids. Mater. Sci. Eng. R Rep. 2002, 36, 1-45. [CrossRef]
- 11. Bhushan, B. Contact mechanics of rough surfaces in tribology: Single asperity contact. *Appl. Mech. Rev.* **1996**, 49, 275–298. [CrossRef]
- 12. Jean, M. The non-smooth contact dynamics method. Comput. Methods Appl. Mech. Eng. 1999, 177, 235–257. [CrossRef]
- 13. Tichy, J.A.; Meyer, D.M. Review of solid mechanics in tribology. Int. J. Solids Struct. 2000, 37, 391–400. [CrossRef]
- 14. Persson, B. Rubber friction and tire dynamics. J. Phys. Condens. Matter 2010, 23, 015003. [CrossRef]
- 15. Gravante, G.; Dell'Annunziata, G.N.; Barbaro, M.; Farroni, F. Experimental Methodology for Tire Ride Analysis Based on Outdoor Cleat Testing. SAE Int. J. Veh. Dyn. Stab. NVH 2025, 9, 357–376. [CrossRef]
- 16. Ghaednia, H.; Wang, X.; Saha, S.; Xu, Y.; Sharma, A.; Jackson, R.L. A review of elastic–plastic contact mechanics. *Appl. Mech. Rev.* **2017**, *69*, 060804. [CrossRef]
- 17. Jackson, R.L.; Ghaednia, H.; Lee, H.; Rostami, A.; Wang, X. Contact mechanics. In *Tribology for Scientists and Engineers: From Basics to Advanced Concepts*; Springer: New York, NY, USA, 2013; pp. 93–140.
- 18. Goryacheva, I.G. Contact Mechanics in Tribology; Springer Science & Business Media: Berlin/Heidelberg, Germany, 2013; Volume 61.
- 19. Zhang, S.; Li, D.; Liu, Y. Friction behavior of rough surfaces on the basis of contact mechanics: A review and prospects. *Micromachines* **2022**, *13*, 1907. [CrossRef] [PubMed]
- 20. Popov, V.L. Contact Mechanics and Friction; Springer: Berlin/Heidelberg, Germany, 2010.
- 21. Popov, V.L.; Heß, M.; Willert, E. *Handbook of Contact Mechanics: Exact Solutions of Axisymmetric Contact Problems*; Springer Nature: Berlin/Heidelberg, Germany, 2019.
- 22. Raous, M.; Jean, M.; Moreau, J.J. Contact Mechanics; Plenum Press: New York, NY, USA, 1995.
- 23. Gilardi, G.; Sharf, I. Literature survey of contact dynamics modelling. Mech. Mach. Theory 2002, 37, 1213–1239. [CrossRef]
- 24. Eid, H.; Pamp, A. An Introductory Overview of Contact Mechanics and Adhesion; Springer: Berlin/Heidelberg, Germany, 2006.
- 25. Ciavarella, M.; Joe, J.; Papangelo, A.; Barber, J. The role of adhesion in contact mechanics. *J. R. Soc. Interface* **2019**, *16*, 20180738. [CrossRef]
- 26. Fischer-Cripps, A.C. Introduction to Contact Mechanics; Springer: New York, NY, USA, 2000.
- 27. Johnson, K. Mechanics of adhesion. Tribol. Int. 1998, 31, 413–418. [CrossRef]
- 28. Roberts, A.D. Rubber contact phenomena. Rubber Chem. Technol. 2014, 87, 383–416. [CrossRef]
- 29. Dubois, G.; Cesbron, J.; Yin, H.P.; Anfosso-Lédée, F. Numerical evaluation of tyre/road contact pressures using a multi-asperity approach. *Int. J. Mech. Sci.* **2012**, *54*, 84–94. [CrossRef]
- 30. Schallamach, A. Friction and abrasion of rubber. Wear 1958, 1, 384–417. [CrossRef]
- 31. Müser, M.H.; Dapp, W.B.; Bugnicourt, R.; Sainsot, P.; Lesaffre, N.; Lubrecht, T.A.; Persson, B.N.; Harris, K.; Bennett, A.; Schulze, K.; et al. Meeting the contact-mechanics challenge. *Tribol. Lett.* **2017**, *65*, 118. [CrossRef]
- 32. Mao, K.; Sun, Y.; Bell, T. Contact mechanics of engineering surfaces: State of the art. Surf. Eng. 1994, 10, 297–306. [CrossRef]
- 33. Hertz, H. Über die Berührung fester elastischer Körper. J. Reine Angew. Math. 1881, 92, 156.
- 34. Fischer-Cripps, A. The Hertzian contact surface. J. Mater. Sci. 1999, 34, 129–137. [CrossRef]
- 35. Johnson, K.L. One hundred years of Hertz contact. Proc. Inst. Mech. Eng. 1982, 196, 363–378. [CrossRef]

36. Wang, Q.J.; Zhu, D. Hertz theory: Contact of spherical surfaces. In *Encyclopedia of Tribology*; Springer: Boston, MA, USA, 2013; pp. 1654–1662.

- 37. Tripp, J.H. *Hertzian Contact in Two and Three Dimensions*; National Aeronautics and Space Administration, Scientific and Technical Information Branch: Washington, DC, USA, 1985.
- 38. Etter, J. Tutorial Report on Hertzian Contact Stress Theory; University of Arizona: Tucson, AZ, USA, 2000.
- 39. Purushothaman, P.; Thankachan, P.; John, S.; Purushothaman, M. Hertz contact stress analysis and validation using finite element analysis. *Int. J. Res. Appl. Sci. Eng. Technol.* **2014**, *2*, 531–538.
- 40. Dintwa, E.; Tijskens, E.; Ramon, H. On the accuracy of the Hertz model to describe the normal contact of soft elastic spheres. *Granul. Matter* **2008**, *10*, 209–221. [CrossRef]
- 41. Sneddon, I.N. The relation between load and penetration in the axisymmetric Boussinesq problem for a punch of arbitrary profile. *Int. J. Eng. Sci.* **1965**, *3*, 47–57. [CrossRef]
- 42. Galin, L. Kontakn'e Zadachi Teorii Uprugosti; Gosudarstvennoe Izdatel'stvo Tekhniko-Teoreticheskoi Literatury: Moscow, Russia, 1953.
- 43. Bhushan, B. Contact mechanics of rough surfaces in tribology: Multiple asperity contact. Tribol. Lett. 1998, 4, 1–35. [CrossRef]
- 44. Taylor, R.I. Rough surface contact modelling—A review. Lubricants 2022, 10, 98. [CrossRef]
- 45. Majumdar, A.; Bhushan, B. Characterization and modeling of surface roughness and contact mechanics. In *Handbook of Micro/Nano Tribology*; CRC Press: Boca Raton, FL, USA, 1995; pp. 109–165.
- 46. Sofonea, M.; Matei, A. Mathematical Models in Contact Mechanics; Cambridge University Press: Cambridge, UK, 2012.
- 47. Bowden, F.P.; Tabor, D. The area of contact between stationary and moving surfaces. *Proc. R. Soc. Lond. Ser. A Math. Phys. Sci.* 1939, 169, 391–413.
- 48. Bowden, F.; Tabor, D. Friction, lubrication and wear: A survey of work during the last decade. *Br. J. Appl. Phys.* **1966**, *17*, 1521. [CrossRef]
- 49. Bowden, F.P.; Tabor, D. The Friction and Lubrication of Solids; Oxford University Press: Oxford, UK, 2001; Volume 1.
- 50. Tabor, D. Friction, surface science and tribology—A personal view. *Proc. Inst. Mech. Eng. Part C Mech. Eng. Sci.* **1991**, 205, 365–378. [CrossRef]
- 51. Carbone, G.; Bottiglione, F. Contact mechanics of rough surfaces: A comparison between theories. *Meccanica* **2011**, *46*, 557–565. [CrossRef]
- 52. Archard, J. Contact and rubbing of flat surfaces. J. Appl. Phys. 1953, 24, 981–988. [CrossRef]
- 53. Archard, J. Elastic deformation and the laws of friction. Proc. R. Soc. Lond. Ser. A Math. Phys. Sci. 1957, 243, 190-205.
- 54. Archard, J. Single contacts and multiple encounters. J. Appl. Phys. 1961, 32, 1420–1425. [CrossRef]
- 55. Emami, A.; Khaleghian, S.; Taheri, S. Asperity-based modification on theory of contact mechanics and rubber friction for self-affine fractal surfaces. *Friction* **2021**, *9*, 1707–1725. [CrossRef]
- 56. Adams, G.G.; Mu" ftu", S.; Azhar, N.M. A scale-dependent model for multi-asperity contact and friction. *J. Tribol.* **2003**, 125, 700–708. [CrossRef]
- 57. Popov, V.L.; Dimaki, A.; Psakhie, S.; Popov, M. On the role of scales in contact mechanics and friction between elastomers and randomly rough self-affine surfaces. *Sci. Rep.* **2015**, *5*, 11139. [CrossRef]
- 58. Hanaor, D.A.; Gan, Y.; Einav, I. Contact mechanics of fractal surfaces by spline assisted discretisation. *Int. J. Solids Struct.* **2015**, *59*, 121–131. [CrossRef]
- 59. Buzio, R.; Boragno, C.; Biscarini, F.; Buatier De Mongeot, F.; Valbusa, U. The contact mechanics of fractal surfaces. *Nat. Mater.* **2003**, *2*, 233–236. [CrossRef]
- 60. Borodich, F.M. Fractal contact mechanics. In Encyclopedia of Tribology; Springer: Boston, MA, USA, 2013; pp. 1249–1258.
- 61. Majumdar, A.; Bhushan, B. Role of fractal geometry in roughness characterization and contact mechanics of surfaces. *J. Tribol.* **1990**, *112*, 205–216. [CrossRef]
- 62. Greenwood, J.A.; Williamson, J.P. Contact of nominally flat surfaces. Proc. R. Soc. Lond. Ser. A Math. Phys. Sci. 1966, 295, 300–319.
- 63. Bush, A.; Gibson, R.; Thomas, T. The elastic contact of a rough surface. Wear 1975, 35, 87–111. [CrossRef]
- 64. Ciavarella, M.; Greenwood, J.; Paggi, M. Inclusion of "interaction" in the Greenwood and Williamson contact theory. *Wear* **2008**, 265, 729–734. [CrossRef]
- 65. Ciavarella, M.; Delfine, V.; Demelio, G. A "re-vitalized" Greenwood and Williamson model of elastic contact between fractal surfaces. *J. Mech. Phys. Solids* **2006**, *54*, 2569–2591. [CrossRef]
- 66. Adams, G.; Nosonovsky, M. Contact modeling—Forces. Tribol. Int. 2000, 33, 431-442. [CrossRef]
- 67. Yakovenko, A.A.; Goryacheva, I.G. Analysis of the discrete contact characteristics based on the Greenwood-Williamson model and the localization principle. *Friction* **2024**, *12*, 1042–1056. [CrossRef]
- 68. Ciavarella, M.; Leoci, F. An assessment of the Greenwood-Williamson and other asperities models, with special reference to electrical conductance. *J. Tribol.* **2006**, *128*, 10–17. [CrossRef]

Appl. Sci. 2025, 15, 11558 23 of 26

69. Farroni, F.; Stefanelli, R.; Dell'Annunziata, G.N.; Timpone, F. Impact of the tire/road local contact area on tire friction, with a novel approach based on Greenwood-Williamson theory and validation in both laboratory and outdoor racing environments. *Tribol. Int.* 2025, 210, 110772. [CrossRef]

- 70. Zhao, T.; Feng, Y. Extended Greenwood–Williamson models for rough spheres. J. Appl. Mech. 2018, 85, 101007. [CrossRef]
- 71. Li, C.Y.; Ding, Y.; Liang, X.M.; Wang, G.F. An improved elastic–plastic contact model with asperity interactions based on Greenwood–Williamson theory. *Acta Mech.* **2023**, 234, 5187–5201. [CrossRef]
- 72. McWaid, T.; Marschall, E. Application of the modified Greenwood and Williamson contact model for the prediction of thermal contact resistance. *Wear* **1992**, 152, 263–277. [CrossRef]
- 73. Jones, R.E. A Greenwood-Williamson model of small-scale friction. J. Appl. Mech. 2007, 74, 31–40. [CrossRef]
- 74. Bush, A.; Gibson, R.; Keogh, G. The limit of elastic deformation in the contact of rough surfaces. *Mech. Res. Commun.* **1976**, 3, 169–174. [CrossRef]
- 75. Zhao, Y.P.; Wang, L.; Yu, T. Mechanics of adhesion in MEMS—A review. J. Adhes. Sci. Technol. 2003, 17, 519–546. [CrossRef]
- 76. Persson, B.N.; Albohr, O.; Tartaglino, U.; Volokitin, A.I.; Tosatti, E. On the nature of surface roughness with application to contact mechanics, sealing, rubberfriction and adhesion. *J. Phys. Condens. Matter* **2004**, *17*, R1. [CrossRef]
- 77. Popov, V.L.; Li, Q.; Lyashenko, I.A. Contact mechanics and friction: Role of adhesion. Friction 2025, 13, 9440964. [CrossRef]
- 78. Marshall, S.J.; Bayne, S.C.; Baier, R.; Tomsia, A.P.; Marshall, G.W. A review of adhesion science. *Dent. Mater.* **2010**, *26*, e11–e16. [CrossRef]
- 79. Adamson, A.W.; Gast, A.P. Physical Chemistry of Surfaces; Interscience Publishers: New York, NY, USA, 1967; Volume 150.
- 80. Lee, L.H. Fundamentals of Adhesion; Springer Science & Business Media: Berlin/Heidelberg, Germany, 2013.
- 81. Bhushan, B. Adhesion and stiction: Mechanisms, measurement techniques, and methods for reduction. *J. Vac. Sci. Technol. B Microelectron. Nanometer Struct. Processing, Meas. Phenom.* **2003**, 21, 2262–2296. [CrossRef]
- 82. Kendall, K.; Roberts, A. van der Waals forces influencing adhesion of cells. *Philos. Trans. R. Soc. B Biol. Sci.* **2015**, *370*, 20140078. [CrossRef]
- 83. Roberts, A. A guide to estimating the friction of rubber. Rubber Chem. Technol. 1992, 65, 673–686. [CrossRef]
- 84. Kendall, K. Adhesion: Molecules and mechanics. Science 1994, 263, 1720–1725. [CrossRef]
- 85. Bradley, R.S. LXXIX. The cohesive force between solid surfaces and the surface energy of solids. *Lond. Edinb. Dublin Philos. Mag. J. Sci.* 1932, 13, 853–862. [CrossRef]
- 86. Nakajima, Y. Advanced Tire Mechanics; Springer: Berlin/Heidelberg, Germany, 2019.
- 87. Schultz, J.; Nardin, M. Theories and mechanisms of adhesion. Mater. Eng. N. Y. 1999, 14, 1–26.
- 88. Packham, D. The mechanical theory of adhesion. In *Handbook of Adhesive Technology*; CRC Press: Boca Raton, FL, USA, 2003; pp. 69–93.
- 89. Johnson, K.L.; Kendall, K.; Roberts, A. Surface energy and the contact of elastic solids. *Proc. R. Soc. Lond. A Math. Phys. Sci.* **1971**, 324, 301–313.
- 90. Derjaguin, B.V.; Muller, V.M.; Toporov, Y.P. Effect of contact deformations on the adhesion of particles. *J. Colloid Interface Sci.* **1975**, 53, 314–326. [CrossRef]
- 91. Barthel, E. Adhesive elastic contacts: JKR and more. J. Phys. D Appl. Phys. 2008, 41, 163001. [CrossRef]
- 92. Hui, C.Y.; Baney, J.; Kramer, E. Contact mechanics and adhesion of viscoelastic spheres. Langmuir 1998, 14, 6570–6578. [CrossRef]
- 93. Coetzee, C. Simplified johnson-kendall-roberts (sjkr) contact model. In *University of Stellenbosch Report*; University of Stellenbosch: Stellenbosch, South Africa, 2020.
- 94. Charrault, E.; Gauthier, C.; Marie, P.; Schirrer, R. Experimental and theoretical analysis of a dynamic JKR contact. *Langmuir* **2009**, 25, 5847–5854. [CrossRef]
- 95. Johnson, K. The adhesion of two elastic bodies with slightly wavy surfaces. Int. J. Solids Struct. 1995, 32, 423–430. [CrossRef]
- 96. Pashley, M. Further consideration of the DMT model for elastic contact. Colloids Surf. 1984, 12, 69–77. [CrossRef]
- 97. Violano, G.; Demelio, G.P.; Afferrante, L. On the DMT adhesion theory: From the first studies to the modern applications in rough contacts. *Procedia Struct. Integr.* **2018**, *12*, 58–70. [CrossRef]
- 98. Violano, G.; Afferrante, L. On DMT methods to calculate adhesion in rough contacts. Tribol. Int. 2019, 130, 36–42. [CrossRef]
- 99. Greenwood, J. On the DMT theory. Tribol. Lett. 2007, 26, 203–211. [CrossRef]
- 100. Prokopovich, P.; Perni, S. Comparison of JKR-and DMT-based multi-asperity adhesion model: Theory and experiment. *Colloids Surf. A Physicochem. Eng. Asp.* **2011**, *383*, 95–101. [CrossRef]
- 101. Tabor, D. Surface forces and surface interactions. In *Plenary and Invited Lectures*; Elsevier: Amsterdam, The Netherlands, 1977; pp. 3–14.
- 102. Muller, V.; Yushchenko, V.; Derjaguin, B. On the influence of molecular forces on the deformation of an elastic sphere and its sticking to a rigid plane. *J. Colloid Interface Sci.* **1980**, 77, 91–101. [CrossRef]
- 103. Maugis, D. Adhesion of spheres: The JKR-DMT transition using a Dugdale model. *J. Colloid Interface Sci.* **1992**, 150, 243–269. [CrossRef]

Appl. Sci. 2025, 15, 11558 24 of 26

- 104. Zhang, Y. Transitions between different contact models. J. Adhes. Sci. Technol. 2008, 22, 699-715.
- 105. Maugis, D.; Gauthier-Manuel, B. JKR-DMT transition in the presence of a liquid meniscus. *J. Adhes. Sci. Technol.* **1994**, *8*, 1311–1322. [CrossRef]
- 106. Maugis, D. The JKR-DMT transition in the presence of a liquid meniscus and the extension of the JKR theory to large contact radii. In *Contact Mechanics*; Springer: Boston, MA, USA, 1995; pp. 335–342.
- 107. Maugis, D. On the contact and adhesion of rough surfaces. J. Adhes. Sci. Technol. 1996, 10, 161–175. [CrossRef]
- 108. Maugis, D. Contact, Adhesion and Rupture of Elastic Solids; Springer Science & Business Media: Berlin/Heidelberg, Germany, 2000; Volume 130.
- 109. Shi, X.; Zhao, Y.P. Comparison of various adhesion contact theories and the influence of dimensionless load parameter. *J. Adhes. Sci. Technol.* **2004**, *18*, 55–68. [CrossRef]
- 110. Ramakrishna, S.N.; Nalam, P.C.; Clasohm, L.Y.; Spencer, N.D. Study of adhesion and friction properties on a nanoparticle gradient surface: Transition from JKR to DMT contact mechanics. *Langmuir* 2013, 29, 175–182. [CrossRef]
- 111. Carbone, G.; Lorenz, B.; Persson, B.N.; Wohlers, A. Contact mechanics and rubber friction for randomly rough surfaces with anisotropic statistical properties. *Eur. Phys. J. E* **2009**, 29, 275–284. [CrossRef]
- 112. Scaraggi, M.; Persson, B.N. General contact mechanics theory for randomly rough surfaces with application to rubber friction. *J. Chem. Phys.* **2015**, 143, 224111. [CrossRef]
- 113. Flores, P. Contact mechanics for dynamical systems: A comprehensive review. Multibody Syst. Dyn. 2022, 54, 127–177. [CrossRef]
- 114. Le Gal, A.; Yang, X.; Klüppel, M. Evaluation of sliding friction and contact mechanics of elastomers based on dynamic-mechanical analysis. *J. Chem. Phys.* **2005**, 123, 014704. [CrossRef]
- 115. Kluppel, M.; Heinrich, G. Rubber friction on self-affine road tracks. Rubber Chem. Technol. 2000, 73, 578-606. [CrossRef]
- 116. Lang, A.; Klüppel, M. Influences of temperature and load on the dry friction behaviour of tire tread compounds in contact with rough granite. *Wear* **2017**, *380*, 15–25. [CrossRef]
- 117. Heinrich, G.; Klüppel, M. Rubber friction, tread deformation and tire traction. Wear 2008, 265, 1052–1060. [CrossRef]
- 118. Le Gal, A.; Klüppel, M. Modeling of rubber friction: A quantitative description of the hysteresis and adhesion contribution. In *Constitutive Models for Rubber IV*; Routledge: Oxfordshire, UK, 2017; pp. 509–514.
- 119. Lang, A.; Klüppel, M. Modelling predictions and experimental investigations of rubber friction and tire traction. In Proceedings of the 4th International Tyre Colloquium: Tyre Models for Vehicle Dynamics Analysis, Guildford, UK, 20–21 April 2015; University of Surrey: Guildford, UK, 2015; pp. 228–233.
- 120. Li, L.; Wang, K.C.; Luo, W. Pavement friction estimation based on the Heinrich/Klüppel model. *Period. Polytech. Transp. Eng.* **2016**, 44, 89–96. [CrossRef]
- 121. Lang, A.; Klüppel, M. Temperature and Pressure dependence of the friction properties of tire tread compounds on rough granite. In Proceedings of the KHK 11th Fall Rubber Colloquium, Hannover, Germany, 26–28 November 2014.
- 122. Klüppel, M.; Müller, A.; Le Gal, A.; Heinrich, G.; Continental, A. *Dynamic Contact of Tires Dynamic Contact of Tires with Road Tracks with Road Tracks*; Rubber Division, American Chemical Society: San Francisco, CA, USA, 2003.
- 123. Le Gal, A.; Yang, X.; Klüppel, M. Sliding friction and contact mechanics of elastomers on rough surfaces. In *Analysis and Simulation of Contact Problems*; Springer: Berlin/Heidelberg, Germany, 2006; pp. 253–260.
- 124. Le Gal, A.; Guy, L.; Orange, G.; Bomal, Y.; Klüppel, M. Modelling of sliding friction for carbon black and silica filled elastomers on road tracks. *Wear* 2008, 264, 606–615. [CrossRef]
- 125. Le Gal, A.; Klüppel, M. Investigation and modelling of rubber stationary friction on rough surfaces. *J. Phys. Condens. Matter* **2007**, 20, 015007. [CrossRef]
- 126. Christensen, R.M. Theory of Viscoelasticity; Courier Corporation: North Chelmsford, MA, USA, 2013.
- 127. Lakes, R.S. Viscoelastic Materials; Cambridge University Press: Cambridge, UK, 2009.
- 128. Papazian, H.S. *The Response of Linear Viscoelastic Materials in the Frequency Domain*; The Ohio State University: Columbus, OH, USA, 1961.
- 129. Schapery, R.A. On the characterization of nonlinear viscoelastic materials. Polym. Eng. Sci. 1969, 9, 295–310. [CrossRef]
- 130. Tomanik, E.; Chacon, H.; Teixeira, G. A simple numerical procedure to calculate the input data of Greenwood-Williamson model of asperity contact for actual engineering surfaces. In *Tribology Series*; Elsevier: Amsterdam, The Netherlands, 2003; Volyme 41, pp. 205–215.
- 131. Nayak, P.R. Random process model of rough surfaces. J. Lubr. Technol. 1971, 93, 398-407. [CrossRef]
- 132. Heinrich, G.; Klüppel, M.; Vilgis, T.A. Evaluation of self-affine surfaces and their implication for frictional dynamics as illustrated with a Rouse material. *Comput. Theor. Polym. Sci.* **2000**, *10*, 53–61. [CrossRef]
- 133. Vanormelingen, K.; Degroote, B.; Vantomme, A. Quantitative characterization of the surface morphology using a height difference correlation function. *J. Vac. Sci. Technol. B Microelectron. Nanometer Struct. Process. Meas. Phenom.* **2006**, 24, 725–729. [CrossRef]
- 134. Torbruegge, S.; Wies, B. Characterization of pavement texture by means of height difference correlation and relation to wet skid resistance. *J. Traffic Transp. Eng. (Engl. Ed.)* **2015**, 2, 59–67. [CrossRef]

Appl. Sci. 2025, 15, 11558 25 of 26

135. Landini, G.; Rigaut, J.P. A method for estimating the dimension of asymptotic fractal sets. Bioimaging 1997, 5, 65–70. [CrossRef]

- 136. Persson, B.N. On the theory of rubber friction. Surf. Sci. 1998, 401, 445–454. [CrossRef]
- 137. Persson, B.; Volokitin, A. Rubber friction on smooth surfaces. Eur. Phys. J. E 2006, 21, 69-80. [CrossRef]
- 138. Yang, C.; Persson, B.N. Contact mechanics: Contact area and interfacial separation from small contact to fullcontact. *J. Phys. Condens. Matter* **2008**, *20*, 215214. [CrossRef]
- 139. Persson, B.N. *Sliding Friction: Physical Principles and Applications*; Springer Science & Business Media: Berlin/Heidelberg, Germany, 2013.
- 140. Persson, B.N. Contact mechanics for randomly rough surfaces. Surf. Sci. Rep. 2006, 61, 201–227. [CrossRef]
- 141. Persson, B.N.; Tosatti, E. *Physics of Sliding Friction*; Springer Science & Business Media: Berlin/Heidelberg, Germany, 2013; Volume 311.
- 142. Persson, B.N. Theory of rubber friction and contact mechanics. J. Chem. Phys. 2001, 115, 3840–3861. [CrossRef]
- 143. Persson, B. Adhesion between an elastic body and a randomly rough hard surface. Eur. Phys. J. E 2002, 8, 385–401. [CrossRef]
- 144. Jacobs, T.D.; Junge, T.; Pastewka, L. Quantitative characterization of surface topography using spectral analysis. *Surf. Topogr. Metrol. Prop.* **2017**, *5*, 013001. [CrossRef]
- 145. Lorenz, B.; Persson, B.; Fortunato, G.; Giustiniano, M.; Baldoni, F. Rubber friction for tire tread compound on road surfaces. *J. Phys. Condens. Matter* **2013**, *25*, 095007. [CrossRef]
- 146. Genovese, A.; Farroni, F.; Papangelo, A.; Ciavarella, M. A discussion on present theories of rubber friction, with particular reference to different possible choices of arbitrary roughness cutoff parameters. *Lubricants* **2019**, 7, 85. [CrossRef]
- 147. Sanyal, A. On the Short Wavelength Cutoff Limit in Persson's Hysteresis Friction Theory. J. Tribol. 2026, 148, 014501. [CrossRef]
- 148. Müser, M.H.; Dapp, W.B. The contact mechanics challenge: Problem definition. arXiv 2015, arXiv:1512.02403. [CrossRef]
- 149. Müser, M.H.; Nicola, L. Modeling the surface topography dependence of friction, adhesion, and contact compliance. *MRS Bull.* **2022**, 47, 1221–1228. [CrossRef]
- 150. Farroni, F. Development of a Grip and Thermodynamics Sensitive Tyre/Road Interaction Forces Characterization Procedure Employed in High-Performance Vehicles Simulation; University of Naples Federico" II: Naples, Italy, 2014.
- 151. Pennestrì, E.; Rossi, V.; Salvini, P.; Valentini, P.P. Review and comparison of dry friction force models. *Nonlinear Dyn.* **2016**, *83*, 1785–1801. [CrossRef]
- 152. Van Der Steen, R. Tyre/Road Friction Modeling: Literature Survey; Eindhoven University of Technology: Eindhoven, The Netherlands, 2007.
- 153. Persson, B.; Xu, R. Rubber Friction: Theory, Mechanisms, and Challenges. arXiv 2025, arXiv:2507.18782. [CrossRef]
- 154. KUMMER, H.W. Rubber and Tire Friction; The Pennsylvania State University: University Park, PA, USA, 1965.
- 155. Smith, R.H. Analyzing Friction in the Design of Rubber Products and Their Paired Surfaces; CRC Press: Boca Raton, FL, USA, 2008.
- 156. Greenwood, J.; Minshall, H.; Tabor, D. Hysteresis losses in rolling and sliding friction. *Proc. R. Soc. Lond. Ser. A Math. Phys. Sci.* **1961**, 259, 480–507.
- 157. Moore, D.; Geyer, W. A review of hysteresis theories for elastomers. Wear 1974, 30, 1–34. [CrossRef]
- 158. Heinrich, G. Hysteresis friction of sliding rubbers on rough and fractal surfaces. Rubber Chem. Technol. 1997, 70, 1–14. [CrossRef]
- 159. Wojewoda, J.; Stefański, A.; Wiercigroch, M.; Kapitaniak, T. Hysteretic effects of dry friction: Modelling and experimental studies. *Philos. Trans. R. Soc. A Math. Phys. Eng. Sci.* **2008**, *366*, 747–765. [CrossRef]
- 160. McFarlane, J.; Tabor, D. Relation between friction and adhesion. Proc. R. Soc. Lond. Ser. A Math. Phys. Sci. 1950, 202, 244–253.
- 161. Chernyak, Y.B.; Leonov, A. On the theory of the adhesive friction of elastomers. Wear 1986, 108, 105–138. [CrossRef]
- 162. Zeng, H. Polymer Adhesion, Friction, and Lubrication; Wiley: Hoboken, NJ, USA, 2013.
- 163. Landheer, D.; De Gee, A. Adhesion, friction, and wear. MRS Bull. 1991, 16, 36-40. [CrossRef]
- 164. Chaudhury, M.K.; Owen, M.J. Adhesion hysteresis and friction. Langmuir 1993, 9, 29-31. [CrossRef]
- 165. Israelachvili, J.N.; Chen, Y.L.; Yoshizawa, H. Relationship between adhesion and friction forces. *J. Adhes. Sci. Technol.* **1994**, *8*, 1231–1249. [CrossRef]
- 166. Popov, V.L. Adhesive contribution to friction. In Proceedings of the International Conference on Advanced Materials with Hierarchical Structure for New Technologies and Reliable Structures 2019, Tomsk, Russia, 1–5 October 2019; AIP Publishing LLC: Melville, NY, USA, 2019; Volume 2167, p. 020286.
- 167. Savkoor, A. On the friction of rubber. Wear 1965, 8, 222–237. [CrossRef]
- 168. Persson, B.N.; Tosatti, E. Qualitative theory of rubber friction and wear. J. Chem. Phys. 2000, 112, 2021–2029. [CrossRef]
- 169. Moore, D.F. Friction and wear in rubbers and tyres. Wear 1980, 61, 273–282. [CrossRef]
- 170. Grosch, K. The relation between the friction and visco-elastic properties of rubber. *Proc. R. Soc. Lond. Ser. A Math. Phys. Sci.* **1963**, 274, 21–39.
- 171. Grosch, K. The rolling resistance, wear and traction properties of tread compounds. *Rubber Chem. Technol.* **1996**, *69*, 495–568. [CrossRef]
- 172. Grosch, K. Rubber friction and tire traction. In *The Pneumatic Tire*; 2006; p. 421. Available online: https://andrzejdebowski.wat.edu.pl/include/wiedza/kolo-ogumione/The%20Pneumatic%20Tire%20NHTSA.pdf (accessed on 27 October 2025).

Appl. Sci. 2025, 15, 11558 26 of 26

173. Grosch, K. Visco-elastic properties and the friction of solids: Relation between the friction and visco-elastic properties of rubber. *Nature* **1963**, *197*, 858–859. [CrossRef]

- 174. Williams, M.L.; Landel, R.F.; Ferry, J.D. The temperature dependence of relaxation mechanisms in amorphous polymers and other glass-forming liquids. *J. Am. Chem. Soc.* **1955**, 77, 3701–3707. [CrossRef]
- 175. Dagdug, L.; García-Colín, L. Generalization of the Williams–Landel–Ferry equation. *Phys. A Stat. Mech. Its Appl.* **1998**, 250, 133–141. [CrossRef]
- 176. Williams, M.L.; Ferry, J.D. Second approximation calculations of mechanical and electrical relaxation and retardation distributions. *J. Polym. Sci.* **1953**, *11*, 169–175. [CrossRef]
- 177. Hertz, H. Miscellaneous Papers; Macmillan: New York, NY, USA, 1896.
- 178. Le Gal, A. Investigation and modelling of adhesion friction on rough surfaces. Kautshcuk Gummi Kunststoffe 2006, 59, 308.
- 179. Persson, B.; Brener, E. Crack propagation in viscoelastic solids. *Phys. Rev. E—Stat. Nonlinear Soft Matter Phys.* **2005**, 71, 036123. [CrossRef]
- 180. Ciavarella, M. A simplified version of Persson's multiscale theory for rubber friction due to viscoelastic losses. *J. Tribol.* **2018**, 140, 011403. [CrossRef]
- 181. Persson, B.N. Rubber friction: Role of the flash temperature. J. Phys. Condens. Matter 2006, 18, 7789. [CrossRef]
- 182. Carbone, G.; Persson, B. Crack motion in viscoelastic solids: The role of the flash temperature. *Eur. Phys. J. E* **2005**, *17*, 261–281. [CrossRef]
- 183. Persson, B. Role of frictional heating in rubber friction. Tribol. Lett. 2014, 56, 77–92. [CrossRef]
- 184. Palade, L.; Verney, V.; Attane, P. Time-temperature superposition and linear viscoelasticity of polybutadienes. *Macromolecules* **1995**, *28*, 7051–7057. [CrossRef]
- 185. Schallamach, A. How does rubber slide? Wear 1971, 17, 301–312. [CrossRef]
- 186. Tolpekina, T.; Pyckhout-Hintzen, W.; Persson, B. Linear and nonlinear viscoelastic modulus of rubber. *Lubricants* **2019**, *7*, 22. [CrossRef]
- 187. Genovese, A.; Carputo, F.; Ciavarella, M.; Farroni, F.; Papangelo, A.; Sakhnevych, A. Analysis of multiscale theories for viscoelastic rubber friction. In Proceedings of the Conference of the Italian Association of Theoretical and Applied Mechanics, Rome, Italy, 15–19 September 2019; Springer: Cham, Switzerland, 2019; pp. 1125–1135.
- 188. Fina, E.; Gruber, P.; Sharp, R. Hysteretic rubber friction: Application of Persson's theories to Grosch's experimental results. *J. Appl. Mech.* **2014**, *81*, 121001. [CrossRef]
- 189. Furlan, M.; Mavros, G. A neural network approach for roughness-dependent update of tyre friction. *Simul. Model. Pract. Theory* **2022**, *116*, 102484. [CrossRef]

Disclaimer/Publisher's Note: The statements, opinions and data contained in all publications are solely those of the individual author(s) and contributor(s) and not of MDPI and/or the editor(s). MDPI and/or the editor(s) disclaim responsibility for any injury to people or property resulting from any ideas, methods, instructions or products referred to in the content.